Spontaneous synchronization in a Josephson transmission line

D. Tsygankov and K. Wiesenfeld
School of Physics, Georgia Institute of Technology, Atlanta, Georgia 30332
(Received 26 April 2002; published 23 September 2002)

At high frequencies, the dynamics of a Josephson array shows fundamental differences from its low-frequency behavior. We consider a simple array where the high-frequency effects are dominant, a current biased series array without any external load. Despite the absence of a load, the oscillators are dynamically coupled at high frequencies, and synchronized states can be attracting. We investigate the character and stability of the synchronized states.

DOI: 10.1103/PhysRevE.66.036215 PACS number(s): 05.45.Xt, 84.40.Az, 74.50.+r

I. INTRODUCTION

The study of synchronization in populations of nonlinear oscillators is one of the best developed areas of nonlinear dynamics of many degree of freedom systems. The field remains very active, as new variations of the problem are explored. The general development of the subject has proceeded along two complementary tracks. One track considers abstract generic models and variations thereof, the Kuramoto model being the most famous (and important) of this type [1]. The other track considers particular physical systems. Prominent among these are the Josephson arrays, that, as a class, provide a varied set of examples to explore.

The motivation for studying Josephson arrays is twofold. On the one hand they have interesting fundamental properties, including a surprising integrability [2] typically found only in Hamiltonian systems; they were also shown to provide a direct physical realization of the Kuramoto model [3]. There is also a practical motivation. These superconducting arrays can operate at extremely high frequencies (up to about a terahertz) and are therefore of interest as amplifiers and sources of electromagnetic radiation in the submillimeter regime [4]. For most applications, these arrays would be useful only if the junctions mutually frequency and phase lock into a dynamical state with a high degree of coherence.

The technological motivation inevitably drives one to consider ever higher operating frequencies and larger arrays. However, in this limit there is a breakdown of the circuit laws typically used to derive the governing dynamical equations [5]. In fact, experiments that have reported on the highest power levels were operating in this regime [6,7]. Other experiments have dramatically illustrated the need to include the distributed nature of high-frequency arrays, by direct comparison of arrays that behave quite differently but have the same lumped circuit description [8].

Despite its importance, our present theoretical understanding of synchronization in the high-frequency regime is relatively primitive. Detailed spatiotemporal information is unavailable from experiments on real Josephson arrays; analog simulations of one or another Josephson system have provided some insight as compared to numerical simulations [8–12]. Models of Josephson junctions coupled to a single-mode resonant cavity, which picks up some of the character of the distributed problem, have also been studied [9,13,14].

The goal of the present work is to make some fundamental progress towards understanding spontaneous synchronization dynamics in a Josephson array. To this end, we consider a simple physical realization: a current biased transmission line interrupted by N equally spaced, identical junctions. This is the load-free version of a model introduced in Ref. [8]. In that work, numerical simulations suggested that the transmission line model replicated experimental data in cases where the lumped model did not.

A nice feature of the load-free system is that in the low-frequency limit the junctions are dynamically uncoupled. In this sense, the system is ideally suited for exploring the new dynamical features that emerge only at higher frequencies.

Mathematically, the distributed problem is more difficult to analyze than the corresponding lumped one, since the governing dynamical equations have much lower symmetry. One consequence is the absence of a perfectly synchronized state in which all oscillators have precisely the same output at all times. This raises the question of what dynamical state(s) to track and how high a degree of synchronization can be achieved even in principle.

In this paper, we apply a perturbation technique that has proved very useful in earlier studies on lumped arrays [15,16]. The calculation leads to the identification of the ''most-synchronized'' dynamical state, and we are able to develop an N-dimensional map that we use to explore the stability of this state. We use numerical simulations of the full dynamical system both as a check of the analytic results and as a means of exploring the dynamics where the most-synchronized state is unstable. The simulations reveal a regime of obvious practical interest, where the array is highly synchronized even though the most-synchronized state is unstable.

II. PROBLEM SETUP AND METHOD OF SOLUTION

We begin by setting up the problem and putting it in a form suitable for the method of analysis. The perturbation scheme we use leads to somewhat lengthy algebraic expressions, but since the idea of the calculation and its structure are simple, it is worthwhile to discuss the main features before presenting the detailed calculation.

Consider a wire of length ℓ interrupted by identical Josephson junctions at positions $x_1, x_2, \ldots, x_{n-1}$. A constant bias current I_b is maintained at one end of the line and removed at the other. At low frequencies, the current within the

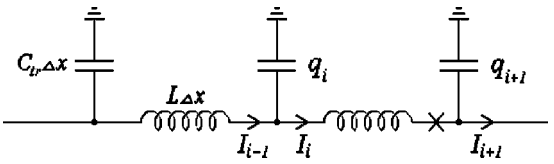

FIG. 1. Finite-element schematic of a piece of the transmission line. The *"X"* denotes a Josephson junction. In the piece shown, only one of the segments contains a junction.

wire is spatially uniform and equal to the value at its ends. At higher frequencies, the wire becomes an active dynamical entity, and can be modeled as a transmission line of inductance L per unit length and capacitance C_{tr} per unit length.

The partial differential equation governing the dynamics of the Josephson transmission line can be determined by considering the finite element representation shown in Fig. 1. Each inductor-capacitor segment represents a short length Δx of the wire. Some segments also contain a Josephson junction in series with the inductor. We assume that each junction is small enough that it can be treated as a lumped element, although the system as a whole is spatially extended. Current conservation implies

$$I_{i-1}=\dot{q}_i+I_i, \tag{1}$$

where q_i is the charge on the ith capacitor, I_i is the current in the ith inductor, and the overdot denotes differentiation with respect to time. Equating voltage drops of two paths from node i to ground yields

$$\frac{q_i}{C_{tr}\Delta x}=L\Delta x\dot{I}_i+\frac{q_{i+1}}{C_{tr}\Delta x}+\frac{\hbar}{2e}\dot{\Phi}_j\delta_{i,i_j}, \tag{2}$$

where $\hbar$ is Planck's constant, e is the magnitude of the electronic charge, and Φ_j is the difference in the phase of the macroscopic quantum wave function across the jth junction. The Kronecker delta is used to include the voltage drop across the jth Josephson junction if it happens to appear in segment i of the transmission line; for example, if the 3rd junction appears in the 89th segment, $i_3=89$. Combining Eqs. (1) and (2) gives

$$\frac{I_{i+1}-2I_i+I_{i-1}}{v^2\Delta x^2}=\ddot{I}_i+\frac{\hbar}{2eL\Delta x}\ddot{\Phi}_j\delta_{i,i_j}, \tag{3}$$

where we have used $v^2=1/(LC_{tr})$. Passing to the limit $\Delta x\to 0$ yields an equation for the current $I(x,t)$,

$$\frac{\partial^2 I}{\partial t^2}-v^2\frac{\partial^2 I}{\partial x^2}+\sum_{j=1}^{n-1}\frac{\hbar}{2eL}\ddot{\Phi}_j\delta(x-x_j)=0. \tag{4}$$

The boundary conditions are

$$I(0,t)=I(\ell,t)=I_b.$$

Meanwhile, since the current through the jth junction is $I(x_j,t)$, we have

$$\frac{\hbar C}{2e}\ddot{\Phi}_j+\frac{\hbar}{2eR}\dot{\Phi}_j+I_c\sin\Phi_j=I(x_j,t), \tag{5}$$

where C, R, and I_c are the junction capacitance, resistance, and critical current, respectively.

To put these in dimensionless form, we first make the rescalings

$$t\to\frac{\hbar}{2eRI_c}t,$$

$$I\to I_cI,$$

to get

$$\frac{\partial^2 I}{\partial t^2}-\frac{\hbar^2v^2}{4e^2R^2I_c^2}\frac{\partial^2 I}{\partial x^2}+\sum_{j=1}^{n-1}\frac{\hbar}{2eI_cL}\ddot{\Phi}_j\delta(x-x_j)=0, \tag{6}$$

$$\beta\ddot{\Phi}_j+\dot{\Phi}_j+\sin\Phi_j=I, \tag{7}$$

where $\beta\equiv 2eCI_cR^2/\hbar$. The next step is to turn the partial differential equation into a set of ordinary differential equations by expanding $I(x,t)$ in spatial modes. A convenient choice is to use the eigenfunctions for the unloaded transmission line, so that

$$I=I_b+\sum_{k=1}^{\infty}A_k(t)\sin\left(\frac{\pi kx}{l}\right). \tag{8}$$

It is easy to see that this automatically satisfies the boundary conditions for arbitrary values of the $\{A_k\}$. Expanding the δ function in the same basis,

$$\delta(x-x_j)=\sum_{k=1}^{\infty}\frac{2}{l}\sin\left(\frac{\pi kx_j}{l}\right)\sin\left(\frac{\pi kx}{l}\right), \tag{9}$$

so that Eq. (6) becomes

$$\ddot{A}_k+c^2k^2A_k+\alpha\sum_{j=1}^{n-1}\ddot{\Phi}_j\sin\left(\frac{\pi kx_j}{l}\right)=0 \tag{10}$$

and

$$\beta\ddot{\Phi}_j+\dot{\Phi}_j+\sin\Phi_j=I_b+\sum_{k=1}^{\infty}A_k\sin\left(\frac{\pi kx_j}{l}\right), \tag{11}$$

where $c=\pi\hbar v/2elRI_c$, $\alpha=\hbar/elLI_c$, and A_k, I_b, t, and β are dimensionless.

We are going to construct a perturbation expansion based on the small parameter $b=1/I_b$, so we make one more rescaling: $t\to(1/I_b)t$ and $A_k\to I_bA_k$, so that our governing system of equations becomes

$$\ddot{A}_k+\tilde{c}^2k^2A_k+\tilde{\alpha}\sum_{j=1}^{n-1}\ddot{\Phi}_j\sin\left(\frac{\pi kx_j}{l}\right)=0, \tag{12}$$

$$\tilde{\beta}\ddot{\Phi}_j+\dot{\Phi}_j+b\sin\Phi_j=1+\sum_{k=1}^{\infty}A_k\sin\left(\frac{\pi kx_j}{l}\right), \tag{13}$$

where $\tilde{c}=cb$, $\tilde{\alpha}=\alpha b$, and $\tilde{\beta}=\beta/b$.

We expect the following perturbation method to be consistent if

$$b \ll 1, \tilde{\alpha}, \tilde{\beta}, \tilde{c}^2. \tag{14}$$

Let us estimate these coefficients. Taking typical experimental values of a junction ($I_c \sim 100\ \mu$A, $R \sim 1\ \Omega$, and $C \sim 1$ pF), and of a trasmission line ($l \sim 100\ \mu$m, $L \sim 10^{-8}$ H/m, and $C_{tr} \sim 10^{-8}$F/m, we find that $v = 1/\sqrt{LC_{tr}} \sim 10^8$ m/s, $\beta \sim 0.1$, $\alpha \sim 10$, and $c \sim 10$. Thus, we will use the values $b=0.05$, $\beta=0.5$, and α and c from ~ 10 to ~ 100 when displaying numerical results later on, in keeping with the condition (14). We note in passing that the characteristic frequency of the solution of Eq. (13) is $\omega_o = 2eRI_c/\hbar b \sim 10^{11}$ Hz.

In the following section, we develop an analytic calculation based on a small b expansion. Specifically, we let

$$A_k = A_k^{(0)} + bA_k^{(1)} + b^2 A_k^{(2)} + \cdots, \tag{15}$$

$$\Phi_k = \Phi_k^{(0)} + b\Phi_k^{(1)} + b^2 \Phi_k^{(2)} + \cdots. \tag{16}$$

Since b is the coefficient of the only nonlinear term, the expansion reduces the problem to a set of linear equations, which allows us to get an explicit representation of the solution.

The structure of the solutions is as follows. To lowest order, the junction phases Φ_j increase at a constant rate. In the familiar pendulum analogy for Josephson junctions, this corresponds to pendulums that overturn with uniform angular velocity. To this order, there are no voltage oscillations and the transmission line modes are inactive. The first-order corrections merely introduce oscillations at the overturning frequency. The crucial interactions show up in second order, and govern the stability of the state in which the junction oscillations are synchronized.

In fact, we find a large number of solutions which depend on the initial values of the junction phases, and this allows us to derive an N-dimensional return map involving the N phases, and it is this map that we use to investigate dynamical stability. We note that this map is not a bona fide Poincaré return map since it does not explicitly involve the other phase space coordinates. Nevertheless, we expect it to be a good approximation to the dynamics after an initial transient time, as the other dynamical variables are effectively slaved by the N phase variables. This expectation is borne out by direct comparisons between the analytic solution and numerical simulations of the full set of equations.

III. PERTURBATION ANALYSIS

A. Zeroth order

To lowest order, Eqs. (12) and (13) are

$$\ddot{A}_k^{(0)} + \tilde{c}^2 k^2 A_k^{(0)} + \tilde{\alpha} \sum_{j=1}^{n-1} \ddot{\Phi}_j^{(0)} \sin\left(\frac{\pi k x_j}{l}\right) = 0,$$

$$\tilde{\beta}\ddot{\Phi}_j^{(0)} + \dot{\Phi}_j^{(0)} = 1 + \sum_{k=1}^{\infty} A_k^{(0)} \sin\left(\frac{\pi k x_j}{l}\right).$$

We readily identify the following N-parameter family of steady state solutions where the junction phases overturn at a constant rate:

$$A_k^{(0)} = 0 \quad \text{and} \quad \Phi_j^{(0)} = t + \theta_j,$$

where the θ_j are constants. One might wonder whether there are also uniformly overturning solutions, but with nonzero $A_k^{(0)}$. Indeed, there can be such solutions; for example, if all of the junctions are placed at nodes of a particular spatial mode, say $k=K$, then there are solutions with $A_K(t) \sim \sin(\tilde{c}Kt)$ and all other $A_k = 0$. These solutions persist indefinitely only because we have assumed that the transmission line is perfectly lossless, and for this reason we ignore them in the ensuing analysis. (Including a small amount of damping in the line would result in more complicated expressions later on without any compensating insight.)

B. First order

To first order in b,

$$\ddot{A}_k^{(1)} + \tilde{c}^2 k^2 A_k^{(1)} + \tilde{\alpha} \sum_{j=1}^{n-1} \ddot{\Phi}_j^{(1)} \sin\left(\frac{\pi k x_j}{l}\right) = 0, \tag{17}$$

$$\tilde{\beta}\ddot{\Phi}_j^{(1)} + \dot{\Phi}_j^{(1)} + \sin(t + \theta_j) = \sum_{k=1}^{\infty} A_k^{(1)} \sin\left(\frac{\pi k x_j}{l}\right). \tag{18}$$

We find the solution of Eqs. (17) and (18) in the form

$$A_k^{(1)} = c_k \sin t + d_k \cos t, \tag{19}$$

$$\Phi_k^{(1)} = a_k \sin t + b_k \cos t. \tag{20}$$

We substitute Eqs. (19) and (20) into Eqs. (17) and (18), and in each equation we equate separately the terms proportional to $\sin t$ and $\cos t$. This yields four sets of equations for the coefficients a_j, b_j, c_j, d_j,

$$c_k(1 - \tilde{c}^2 k^2) + \tilde{\alpha} \sum_{j=1}^{n-1} a_j \sin\left(\frac{\pi k x_j}{l}\right) = 0, \tag{21}$$

$$d_k(1 - \tilde{c}^2 k^2) + \tilde{\alpha} \sum_{j=1}^{n-1} b_j \sin\left(\frac{\pi k x_j}{l}\right) = 0, \tag{22}$$

$$-\tilde{\beta} a_j - b_j + \cos\theta_j = \sum_{k=1}^{\infty} c_k \sin\left(\frac{\pi k x_j}{l}\right), \tag{23}$$

$$-\tilde{\beta} b_j + a_j + \sin\theta_j = \sum_{k=1}^{\infty} d_k \sin\left(\frac{\pi k x_j}{l}\right). \tag{24}$$

Multiplying Eq. (23) by $\tilde{\beta}$ and subtracting the result from Eq. (24) gives, upon solving for a_j,

$$a_j=\frac{1}{1+\tilde{\beta}^2}(\tilde{\beta}\cos\theta_j-\sin\theta_j)+\frac{1}{1+\tilde{\beta}^2}\times\sum_{k=1}^{\infty}(d_k-\tilde{\beta}c_k)\sin\left(\frac{\pi kx_j}{l}\right), \tag{25}$$

whereas multiplying Eq. (24) by $\tilde{\beta}$ and adding the result to Eq. (23) leads to an expression for b_j,

$$b_j=\frac{1}{1+\tilde{\beta}^2}(\tilde{\beta}\sin\theta_j+\cos\theta_j)-\frac{1}{1+\tilde{\beta}^2}\times\sum_{k=1}^{\infty}(\tilde{\beta}d_k+c_k)\sin\left(\frac{\pi kx_j}{l}\right). \tag{26}$$

Let

$$S_{k'k}=\sum_{j=1}^{n-1}\sin\left(\frac{\pi k'x_j}{l}\right)\sin\left(\frac{\pi kx_j}{l}\right).$$

Then substituting Eqs. (25) and (26) into Eqs. (21) and (22) gives

$$c_k(1-\tilde{c}^2k^2)+\frac{\tilde{\alpha}}{1+\tilde{\beta}^2}\sum_{j=1}^{n-1}(\tilde{\beta}\cos\theta_j-\sin\theta_j)\sin\left(\frac{\pi kx_j}{l}\right)+\frac{\tilde{\alpha}}{1+\tilde{\beta}^2}\sum_{k'=1}^{\infty}(d_{k'}-\tilde{\beta}c_{k'})S_{k'k}=0,$$

$$d_k(1-\tilde{c}^2k^2)+\frac{\tilde{\alpha}}{1+\tilde{\beta}^2}\sum_{j=1}^{n-1}(\tilde{\beta}\sin\theta_j+\cos\theta_j)\sin\left(\frac{\pi kx_j}{l}\right)-\frac{\tilde{\alpha}}{1+\tilde{\beta}^2}\sum_{k'=1}^{\infty}(\tilde{\beta}d_{k'}+c_{k'})S_{k'k}=0.$$

So far, our calculation is good for any spatial distribution of junctions. We now specialize to the important case of equally spaced junctions: $x_j=lj/n$, where $j=1,2,\ldots,n-1$. Then $S_{k'k}=(n/2)\delta_{k'k}$ [17], and the last expressions decouple in k. It is then a straightforward matter to solve them, with the results

$$c_k=P\sum_{j=1}^{n-1}\frac{\tilde{\beta}H+M_k}{M_k^2+H^2}\sin\theta_j\sin\left(\frac{\pi kj}{n}\right)+P\sum_{j=1}^{n-1}\frac{H-\tilde{\beta}M_k}{M_k^2+H^2}\cos\theta_j\sin\left(\frac{\pi kj}{n}\right),$$

$$d_k=-P\sum_{j=1}^{n-1}\frac{\tilde{\beta}H+M_k}{M_k^2+H^2}\cos\theta_j\sin\left(\frac{\pi kj}{n}\right)+P\sum_{j=1}^{n-1}\frac{H-\tilde{\beta}M_k}{M_k^2+H^2}\sin\theta_j\sin\left(\frac{\pi kj}{n}\right),$$

where $M_k\equiv1-\tilde{c}^2k^2-\tilde{\beta}H$, $P\equiv2H/n$, and $H\equiv\tilde{\alpha}n/[2(1+\tilde{\beta}^2)]$.

Finally, we substitute this back into Eqs. (25) and (26),

$$a_j=\frac{P}{\tilde{\alpha}}(\tilde{\beta}\cos\theta_j-\sin\theta_j)+\frac{P^2}{\tilde{\alpha}}\sum_{i=1}^{n-1}\sum_{k=1}^{\infty}\frac{H(1-\tilde{\beta}^2)-2\tilde{\beta}M_k}{M_k^2+H^2}\times\sin\theta_i\sin\left(\frac{\pi ki}{n}\right)\sin\left(\frac{\pi kj}{n}\right)-\frac{P^2}{\tilde{\alpha}}\sum_{i=1}^{n-1}\sum_{k=1}^{\infty}\frac{M_k(1-\tilde{\beta}^2)+2\tilde{\beta}H}{M_k^2+H^2}\times\cos\theta_i\sin\left(\frac{\pi ki}{n}\right)\sin\left(\frac{\pi kj}{n}\right),$$

$$b_j=\frac{P}{\tilde{\alpha}}(\tilde{\beta}\sin\theta_j+\cos\theta_j)-\frac{P^2}{\tilde{\alpha}}\sum_{i=1}^{n-1}\sum_{k=1}^{\infty}\frac{H(1-\tilde{\beta}^2)-2\tilde{\beta}M_k}{M_k^2+H^2}\times\cos\theta_i\sin\left(\frac{\pi ki}{n}\right)\sin\left(\frac{\pi kj}{n}\right)-\frac{P^2}{\tilde{\alpha}}\sum_{i=1}^{n-1}\sum_{k=1}^{\infty}\frac{M_k(1-\tilde{\beta}^2)+2\tilde{\beta}H}{M_k^2+H^2}\times\sin\theta_i\sin\left(\frac{\pi ki}{n}\right)\sin\left(\frac{\pi kj}{n}\right).$$

C. Second order

The second-order expansion of Eqs. (12) and (13) gives

$$\ddot{A}_k^{(2)}+\tilde{c}^2k^2A_k^{(2)}+\tilde{\alpha}\sum_{j=1}^{n-1}\ddot{\Phi}_j^{(2)}\sin\left(\frac{\pi kx_j}{l}\right)=0, \tag{27}$$

$$\tilde{\beta}\ddot{\Phi}_j^{(2)}+\dot{\Phi}_j^{(2)}+\cos(t+\theta_j)\Phi_j^{(1)}=\sum_{k=1}^{\infty}A_k^{(2)}\sin\left(\frac{\pi kx_j}{l}\right). \tag{28}$$

Now, the third term on the left hand side is equal to the sum of a constant term plus second-Harmonic terms. Thus, the solution is of the form

$$\Phi_j^{(2)}=-\langle b\cos(t+\theta_j)\Phi_j^{(1)}\rangle t+E_j\sin2t+F_j\cos2t, \tag{29}$$

$$A_k^{(2)}=G_k\sin2t+H_k\cos2t, \tag{30}$$

where the angular brackets denote a time average over one period. In Sec. V, where we consider the stability of solutions, we do not therefore need explicit expressions for the coefficients E_j, F_j, G_j, and H_j. On the other hand, the stability hinges crucially on the coefficient of the term proportional to t, which is

$$\langle \cos(t+\theta_j)\Phi_j^{(1)}\rangle = \frac{1}{2}(b_j\cos\theta_j - a_j\sin\theta_j)$$

$$= \frac{P}{2\tilde{\alpha}} - \frac{P^2}{2\tilde{\alpha}}\sum_{i=1}^{n-1}\sum_{k=1}^{\infty}\frac{H(1-\tilde{\beta}^2)-2\tilde{\beta}M_k}{M_k^2+H^2}$$

$$\times\cos(\theta_j-\theta_i)\sin\left(\frac{\pi ki}{n}\right)\sin\left(\frac{\pi kj}{n}\right)$$

$$+\frac{P^2}{2\tilde{\alpha}}\sum_{i=1}^{n-1}\sum_{k=1}^{\infty}\frac{M_k(1-\tilde{\beta}^2)+2\tilde{\beta}H}{M_k^2+H^2}$$

$$\times\sin(\theta_j-\theta_i)\sin\left(\frac{\pi ki}{n}\right)\sin\left(\frac{\pi kj}{n}\right). \quad (31)$$

IV. THE MOST-SYNCHRONIZED STATE

In this section we explore the characteristics of the obtained solution to first order in b in the case when $\theta_j=\theta$, for all j. As noted previously, our system does not admit the type of fully symmetric in-phase state that is found in many lumped circuit problems. However, the solution with $\theta_j=\theta$ is the ''most-synchronized'' state in the sense that, in the limit $b\to 0$, this is the solution branch that coincides with the in-phase state. As we will see, the wave forms for this state can line up virtually perfectly even though the amplitudes can differ substantially from one oscillator to the next.

It is convenient to introduce the following notation:

$$\sigma_{ij} = P\sum_{k=1}^{\infty}\frac{H(1-\tilde{\beta}^2)-2\tilde{\beta}M_k}{M_k^2+H^2}\sin\left(\frac{\pi ki}{n}\right)\sin\left(\frac{\pi kj}{n}\right), \quad (32)$$

$$\rho_{ij} = P\sum_{k=1}^{\infty}\frac{M_k(1-\tilde{\beta}^2)+2\tilde{\beta}H}{M_k^2+H^2}\sin\left(\frac{\pi ki}{n}\right)\sin\left(\frac{\pi kj}{n}\right). \quad (33)$$

Then we can rewrite the coefficients a_j and b_j in the form

$$a_j = \frac{P}{\tilde{\alpha}}\left[\left(\tilde{\beta}-\sum_{i=1}^{n-1}\rho_{ij}\right)\cos\theta - \left(1-\sum_{i=1}^{n-1}\sigma_{ij}\right)\sin\theta\right], \quad (34)$$

$$b_j = \frac{P}{\tilde{\alpha}}\left[\left(\tilde{\beta}-\sum_{i=1}^{n-1}\rho_{ij}\right)\sin\theta + \left(1-\sum_{i=1}^{n-1}\sigma_{ij}\right)\cos\theta\right]. \quad (35)$$

Note that as $k\to\infty$, the terms in Eqs. (32) and (33) tend to zero as $1/k^2$. Hence, for numerical purposes we can consider finite sums choosing big enough $k_{\max}$ for any required accuracy.

Next, we define an order parameter that represents the degree of synchronization of the array. The quantity of direct physical interest is the voltage across a junction, and this is proportional to $\dot{\Phi}$. To first order in our perturbation expansion, we have

$$\dot{\Phi}_j = 1 + b\dot{\Phi}_j^{(1)} + O(b^2) = 1 + b(a_j\cos t - b_j\sin t) + O(b^2).$$

To study the effects of phase locking, we write this as

$$\dot{\Phi}_j = 1 + be_j\sin(t+f_j) + O(b^2),$$

so that a natural order parameter is

$$p = |\langle\exp(if_j)\rangle| = \left|\frac{1}{(n-1)}\sum_{j=1}^{n-1}\exp(if_j)\right|. \quad (36)$$

We want to express f_j in terms of the derived quantities σ_{ij}, ρ_{ij}. Equating the last two expressions for $\dot{\Phi}_j$ gives

$$f_j = -\arctan\frac{a_j}{b_j}, \quad (37)$$

and so, in view of Eqs. (34) and (35),

$$\tan f_j = \frac{\left(1-\sum_i\sigma_{ij}\right)\sin\theta - \left(\tilde{\beta}-\sum_i\rho_{ij}\right)\cos\theta}{\left(1-\sum_i\sigma_{ij}\right)\cos\theta + \left(\tilde{\beta}-\sum_i\rho_{ij}\right)\sin\theta}$$

$$= \frac{\tan\theta-\tan\tilde{\theta}_j}{1+\tan\theta\tan\tilde{\theta}_j} = \tan(\theta-\tilde{\theta}_i),$$

where for the moment we have introduced the quantity

$$\tan\tilde{\theta}_j = \frac{\tilde{\beta}-\sum_i\rho_{ij}}{1-\sum_i\sigma_{ij}}.$$

Finally, then, we get the desired formula for the phase of the voltage wave form,

$$f_j = \theta - \arctan\frac{\tilde{\beta}-\sum_i\rho_{ij}}{1-\sum_i\sigma_{ij}}. \quad (38)$$

Meanwhile, the amplitude of the voltage wave form is

$$e_j = \sqrt{a_j^2+b_j^2} = \frac{P}{\tilde{\alpha}}\sqrt{\left(\tilde{\beta}-\sum_i\rho_{ij}\right)^2+\left(1-\sum_i\sigma_{ij}\right)^2}. \quad (39)$$

The order parameter, Eq. (36), is unity when all of the voltage wave forms line up and it tends to be zero if the

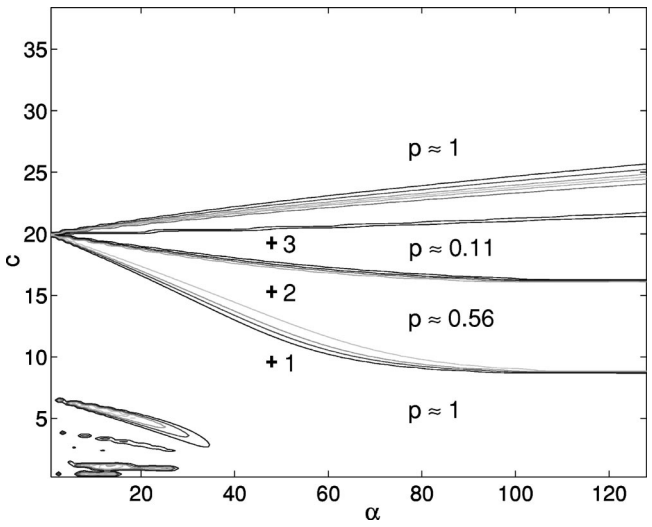

FIG. 2. Contour plot of the order parameter p as a function of α and c using the analytic result, Eq. (36). Here $b=0.05$, $\beta=0.5$, $n=10$, $k_{max}=40$. The symbols 1, 2, and 3 indicate the points of the parameter space that we used for the following Figs. 3, 4, and 5 correspondingly.

wave form phases f_j are randomly distributed on the interval $[-\pi,+\pi]$. Figure 2 shows the dependence of p on α and c. There are regions where the order parameter is approximately 1 (to within a few percent), where it is relatively small (~ 0.1) and where it has intermediate values. Figures 3, 4, and 5 demonstrate the behavior of the solution $\dot{\Phi}_j$ in these different regions of parameter space. Also shown in these figures are the corresponding results generated from direct numerical integration of the nonlinear differential equations (12) and (13). These are in good agreement with the analytically derived solution.

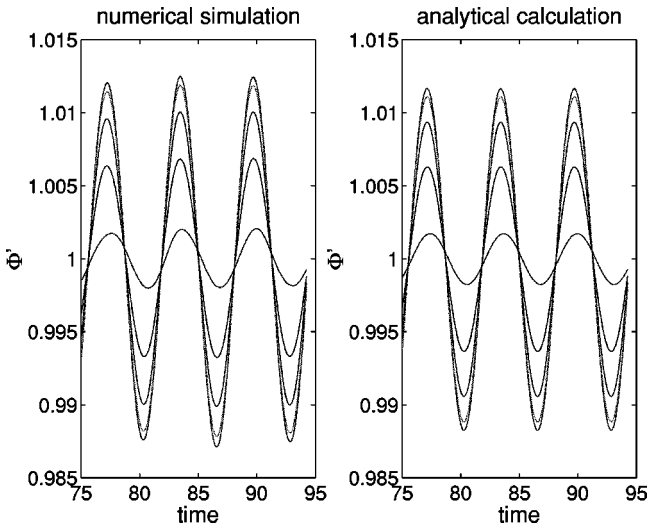

FIG. 3. Functions $\dot{\Phi}_j(t)$ corresponding to the point 1 on Fig. 2 ($\alpha=48, c=9.6$) from the region with $p\approx 1.00$. Although there are nine junctions, only five curves are seen, since the wave forms of junctions symmetrically located about the midpoint are identical.

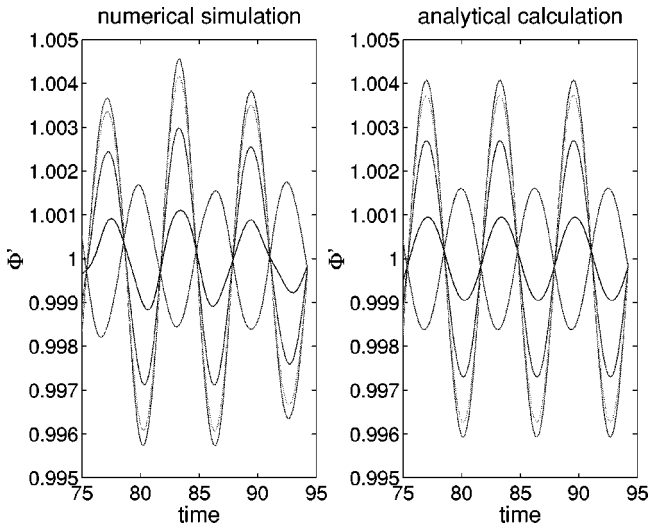

FIG. 4. Functions $\dot{\Phi}_j(t)$ corresponding to the point 2 on Fig. 2 ($\alpha=48$, $c=15.6$) from the region with $p\approx 0.56$.

V. STABILITY OF THE MOST-SYNCHRONIZED STATE

Through second order, the solution for Φ_j is

$$\Phi_j(t)=t+\theta_j+b(a_j\sin t+b_j\cos t)-b^2(\langle\cos(t+\theta_j)\Phi_j^{(1)}\rangle t + E_j\sin 2t+F_j\cos 2t)+O(b^3).$$

Evaluating this at $t=0$ and $t=2\pi$ leads to [cf. Eqs. (31)–(33)]

$$\Phi_j(2\pi)=\Phi_j(0)+2\pi\left(1-\frac{b^2P}{2\tilde{\alpha}}+\frac{b^2P}{2\tilde{\alpha}}\sum_{i=1}^{n-1}\sigma_{ij}\cos[\Phi_j(0)-\Phi_i(0)]-\frac{b^2P}{2\tilde{\alpha}}\sum_{i=1}^{n-1}\rho_{ij}\sin[\Phi_j(0)-\Phi_i(0)]\right),$$

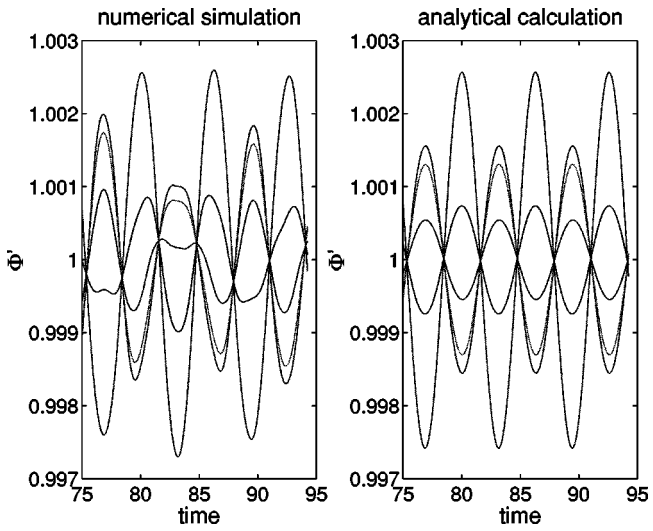

FIG. 5. Functions $\dot{\Phi}_j(t)$ corresponding to the point 3 on Fig. 2 ($\alpha=48$, $c=19.2$) from the region with $p\approx 0.11$.

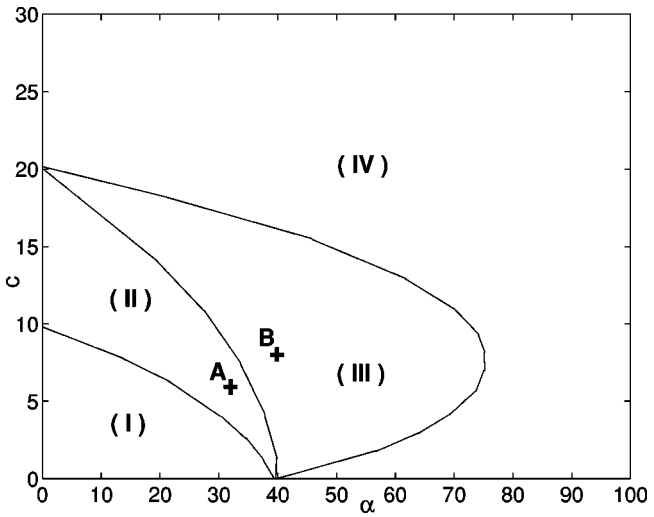

FIG. 6. Schematic (based on the contour plot of the maximum eigenvalue of $\mathbf{T}_{ij}$ as a function of α and c for $b=0.05$, $\beta=0.5$, $n=10$, $k_{max}=40$), identifying qualitatively different regions of parameter space.

where we have used the fact that $\Phi_j(0)=\theta_j+O(b)$. We can view this as an N-dimensional map for the phase dynamics. That it involves ''only'' N variables is significant, since this is much smaller than the phase space dimension of the original problem. In effect, the map treats the other degrees of freedom as being slaved to the junction phases.

Consider now orbits that are infinitesimally close to the ''most-synchronized'' solution we identified previously, so that $\theta_j=\theta+\delta\theta_j$, where $|\delta\theta_j|\ll|\theta|$. Then we get $\Phi_j=\Phi_j^0+\delta\Phi_j$, where

$$\Phi_j^0(2\pi)=\Phi^0(0)+\left(2\pi-\frac{\pi b^2 P}{\tilde{\alpha}}+\frac{\pi b^2 P}{\tilde{\alpha}}\sum_{i=1}^{n-1}\sigma_{ij}\right), \tag{40}$$

$$\delta\Phi_j(2\pi)=\delta\Phi_j(0)-\frac{\pi b^2 P}{\tilde{\alpha}}\sum_{i=1}^{n-1}\rho_{ij}[\delta\Phi_j(0)-\delta\Phi_i(0)], \tag{41}$$

with $\Phi^0(0)=\theta$ and $\delta\Phi_j(0)=\delta\theta_j$. We now ask whether the perturbations grow or shrink. We can rewrite Eq. (41) in matrix form,

$$\delta\vec{\Phi}(2\pi)=\mathbf{T}\delta\vec{\Phi}(0),$$

where

$$\mathbf{T}_{ij}=\delta_{ij}\left(1-\frac{\pi b^2 P}{\tilde{\alpha}}\sum_m \rho_{mj}\right)+\frac{\pi b^2 P}{\tilde{\alpha}}\rho_{ij}. \tag{42}$$

If we denote by r the eigenvalue of this matrix which has the largest magnitude, the stability condition is $r\leqslant 1$.

Figure 6 summarizes the behavior of r over the (α,c)-parameter plane. We can identify four qualitively different regions of parameters space. Region (I) corresponds to a regime where both r and the order parameter p varying in an irregular fashion. This region falls outside the regime where the perturbation expansion is valid, according to the condition (14). Region (II) also corresponds to an unstable regime, with the minimum eigenvalue of $\mathbf{T}_{ij}$ equal to 1 and all the other eigenvalues greater than 1. Region (III) corresponds to a stable regime where the maximum eigenvalue is equal to 1 and all the other eigenvalues are less than 1. Region (IV) also corresponds to a stable regime, but it is qualitatively different from region (III) by virtue of the fact that all of the eigenvalues here are close to 1, so that this is a region of very weak stability.

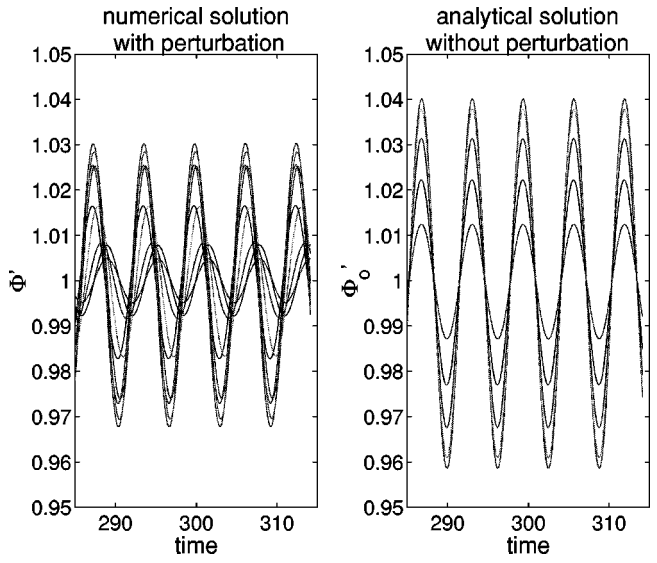

FIG. 7. Functions $\dot{\Phi}_j(t)$ and $\dot{\Phi}_j^0(t)$ corresponding to the point A on Fig. 6 ($\alpha=32$, $c=6.00$; unstable regime).

Figures 7 and 8 demonstrate the behavior of the solution with parameters taken from opposite sides of the stability threshold. Figure 7 corresponds to the point A in region (II), so that the initially perturbed solution never tends to the

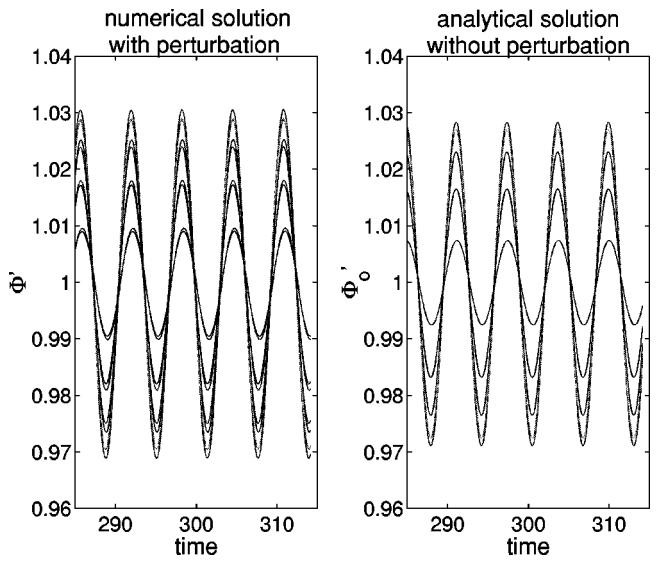

FIG. 8. Functions $\dot{\Phi}_j(t)$ and $\dot{\Phi}_j^0(t)$ corresponding to the point B on Fig. 6 ($\alpha=40$, $c=8.16$; stable regime).

synchronized state $\dot{\Phi}_j^0$. Figure 8 corresponds to the point B in region (III) where the initially perturbed solution converges to the in-phase state.

VI. SUMMARY AND DISCUSSION

Our primary motivation was to develop some fundamental theoretical understanding of the synchronization dynamics when the spatial extent of the array is a significant factor. As a practical matter, this is an important issue if arrays are to produce greater power levels and/or operate at very high frequencies, since in either instance the system gets pushed out of the lumped circuit limit. We have chosen a relatively simple situation to underscore the new physics that ''turns on'' in this regime. By considering a series array without an additional load, we have isolated the new coupling effects; without them (i.e., at low frequencies) the junctions are dynamically uncoupled, and no synchronization—in phase, splay phase or otherwise—is possible.

One property of the distributed system is that the ''perfectly'' synchronized state—the so-called in-phase state—is not a possible solution. This makes the problem more subtle to study than the corresponding load-coupled lumped arrays, where the high degree of symmetry of the in-phase state can be exploited. One nice feature of the perturbation expansion we employed is that it naturally identifies a highly synchronized solution that may be thought of as the continuation of the solution branch containing the in-phase state. It is this state whose properties we analyzed.

Another interesting and somewhat unexpected result is that the array can show significant synchronization even when the most-synchronized state is unstable. The contour plot of Fig. 2 summarizes this aspect of the problem. It is consistent with the stability diagram Fig. 6, and in some respects is equally useful. We also found a large region of parameter space where the most-synchronized state is stable but only very weakly so, and presumably in this regime the coherence would be easily corrupted by the presence of quenched disorder and dynamical noise.

One obviously interesting variation of the problem is to consider spatially clustered junctions, an architecture that experiments have shown can result in significantly higher output powers than arrays in which the junctions are equally spaced [6–8]. This presents a great challenge for the theorist, since a nonuniform spacing of junctions lowers the symmetry of the problem still further. It may be that the problem becomes tractable again for certain spatial patterns; in any event, very little is known theoretically about this problem.

A natural question to ask is whether our results are sensitive to weak disorder. We have presented results only for the case where the junctions are identical and equally spaced. The question of disorder deserves careful and systematic investigation, and we have not undertaken such a study. As a general rule, in regions of parameter space where the synchronized state is attracting, one expects the system behavior to be robust with respect to the addition of at least a small amount of disorder. Indeed, if the attractors are hyperbolic—the usual case except at bifurcation points—we are guaranteed that the attractors persist and vary continuously with arbitrary changes in the parameter values. To test this, we have run numerical simulations for our system [Eqs. (12) and (13)], including a 5% spread in the parameters β_j and x_j, where β_j involves the junction parameters and x_j is the junction position. The behavior is not greatly changed, for example, for the conditions in Fig. 3, the disorder has a negligible effect on phase synchronization, and introduces variations of about 2% in the amplitudes. We might expect the most significant changes to occur at the stability boundary of the synchronized state, and in the region where the synchronized state is (in the ideal case) only weakly stable.

Finally, we point out that the same considerations that motivated the present work also apply to other physical realizations of coupled oscillator arrays. Of particular note are arrays of semiconductor oscillators, which are being used to implement new strategies for power combining, beam steering, and beam shaping [18–20]. These arrays typically operate in the distributed-coupling limit in direct analogy with the Josephson system we studied here. The spatial variations of current in the stripline connecting the array elements acts as an intermediary that couples the various oscillators. Just as in the Josephson problem, the various desirable dynamical states are highly synchronized. An analysis carried out along the lines here could determine which stripline conditions would be most favorable for achieving the target attractors.

ACKNOWLEDGMENT

This work was supported by a grant from the Office of Naval Research under Contract No. N00014-99-1-0592.

[1] Y. Kuramoto, Lect. Notes Phys. **39**, 420 (1975); *Chemical Oscillations, Waves, and Turbulence* (Springer, Berlin, 1984).
[2] S. Watanabe and S.H. Strogatz, Physica D **74**, 197 (1994).
[3] K. Wiesenfeld, P. Colet, and S.H. Strogatz, Phys. Rev. Lett. **76**, 404 (1996); Phys. Rev. E **57**, 1563 (1998).
[4] T. P. Orlando and K. A. Delin, *Foundations of Applied Superconductivity* (Addison-Wesley, Reading, MA, 1991).
[5] K. K. Likharev, *Dynamics of Josephson Junctions and Circuits* (Gordon and Breach, New York, 1986).
[6] S. Han, B. Bi, W. Zhang, and J.E. Lukens, Appl. Phys. Lett. **64**, 1424 (1994).
[7] P.A.A. Booi and S.P. Benz, Appl. Phys. Lett. **68**, 3799 (1996).
[8] A. Cawthorne, C. Lobb, P. Barbara, A. Shitov, K. Wiesenfeld, and A. Zangwill, Phys. Rev. B **60**, 7575 (1999).
[9] E. Almaas and D. Stroud, Phys. Rev. B (to be published).
[10] J. E. Savageau, Ph.D. thesis, SUNY, Stony Brook, 1987.
[11] J.A. Blackburn, H.J.T. Smith, and N. Gronbech-Jensen, J. Appl. Phys. **70**, 2395 (1991).
[12] H.J.T. Smith, J.A. Blackburn, and N. Gronbech-Jensen, J. Appl. Phys. **74**, 5101 (1993).
[13] N. Gronbech-Jensen, R.D. Parmentier, and N.F. Pedersen, Phys. Lett. A **142**, 427 (1989).

[14] G. Filatrella, G. Rotoli, N. Gronbech-Jensen, R.D. Parmentier, and N.F. Pedersen, J. Appl. Phys. **72**, 3179 (1992).
[15] A.A. Chernikov and G. Schmidt, Phys. Rev. E **52**, 3415 (1995).
[16] M. Dhamala and K. Wiesenfeld, Phys. Lett. A **292**, 269 (2002).
[17] This is true only until $2n > \max(k, k')$, which becomes relevant when selecting an acceptable cutoff index in the modal expansion for numerical simulations.
[18] R.A. York, IEEE Trans. Microwave Theory Tech. **41**, 1799 (1993); R.A. York and T. Itoh, *ibid.* **46**, 1920 (1998).
[19] T. Heath, K. Wiesenfeld, and R.A. York, Int. J. Bifurcation Chaos Appl. Sci. Eng. **10**, 2619 (2000).
[20] R.J. Pogorzelski, IEEE Microwave Guid. Wave Lett. **10**, 478 (2000); IEEE Trans. Microwave Theory Tech. **50**, 143 (2002).